Scientific Reports

https://doi.org/10.1038/s41598-026-49187-7

Article in Press

Exploring potential VEGF receptor 2 inhibitors: a molecular modeling and pharmacophore-based screening approach

Received: 9 December 2025

Accepted: 13 April 2026

Published online: 25 April 2026

Cite this article as: Mozzicafreddo M., Benfaremo D., Agarbati S. *et al.* Exploring potential VEGF receptor 2 inhibitors: a molecular modeling and pharmacophore-based screening approach. *Sci Rep* (2026). https://doi.org/10.1038/s41598-026-49187-7

Matteo Mozzicafreddo, Devis Benfaremo, Silvia Agarbati, Carolina Clementi, Chiara Paolini, Silvia Svegliati Baroni & Gianluca Moroncini

Exploring Potential VEGF Receptor 2 Inhibitors: A Molecular Modeling and Pharmacophore-Based Screening Approach

Matteo Mozzicafreddo [1,*], Devis Benfaremo [1,2], Silvia Agarbati [1], Carolina Clementi [1], Chiara Paolini [1], Silvia Svegliati Baroni [1,2] and Gianluca Moroncini [1,2]

[1] Department of Clinical and Molecular Sciences, Marche Polytechnic University, 60126 Ancona, Italy
[2] Clinica Medica, Department of Internal Medicine, Marche University Hospital, 60126 Ancona, Italy

Keywords: VEGF receptor; cancer; fibrosis-related diseases; pharmacophore-based screening; molecular docking; molecular dynamics; quantitative structure–activity relationship; structure-based drug design.

*Corresponding author: Matteo Mozzicafreddo, Department of Clinical and Molecular Sciences, Marche Polytechnic University, 60126 Ancona, Italy.
Email: m.mozzicafreddo@staff.univpm.it

Running title: Pharmacophore-Guided Discovery of VEGFR-2 Inhibitors.

Abstract

The vascular endothelial growth factor (VEGF) receptor 2, a membrane tyrosine kinase receptor activated by VEGF-A, triggers endothelial cell proliferation, migration, survival, and angiogenesis. With the aim of identifying additional new ligands or acquiring novel information to craft potent drugs, the focus of this study was to point to this macromolecule as to a possible target for selective modulators or inhibitors. Using the Pharmit server, pharmacophore-based screening of about 450 million compounds was performed, yielding candidate ligands evaluated through molecular modeling tools such as molecular docking, molecular dynamics, and 3D quantitative structure–activity relationship analysis. The best complex, PubChem-143070699/VEGFR2, matched the proposed pharmacophore model and predicted nanomolar affinity. While experimental evidence remains mandatory to decipher the mechanisms underlying VEGFR2 inhibitors, the predicted structural insights gleaned from this research hold promise for advancing the development of increasingly potent and precisely targeted therapies for VEGFR-associated conditions, such as cancer and fibrosis-related diseases.

Introduction

The vascular endothelial growth factor (VEGF) receptor 2 belongs to the receptor tyrosine kinase (RTK) family and plays a vital role in the growth of blood vessels, whether they are new (vasculogenesis) or pre-existing (angiogenesis). In particular, the VEGF-A/VEGF receptor 2 signaling pathway triggers endothelial cell proliferation, migration, survival, and the formation of new blood vessels [1,2]. To assess the important role of this pathway, Abhinand *et al.* have developed a comprehensive map of endothelial cell-specific signaling events [2]. This map includes 240 proteins and their various post-translational modifications, shedding light on the intricacies of VEGF-A/VEGF receptor 2 signal transduction in angiogenesis.

VEGF receptor (VEGFR) becomes activated upon the attachment of vascular endothelial growth factors (VEGFs) to its extracellular domain, inducing receptor dimerization. This structural alteration exposes the ATP binding site, enabling ATP binding, which in turn triggers tyrosine residue phosphorylation and subsequent activation of the receptor [3-6].

Inhibitors of VEGFR are classified based on receptor conformation and ATP competition. Among these, the second type comprises non-ATP competitors that bind to and stabilize the inactive form of the receptor, known as the aspartic acid/ phenylalanine/glycine (DFG)-out conformer. This stabilization is achieved through a flip of the receptor's DFG motif, which exposes an additional hydrophobic pocket (the allosteric site). The ligand/inhibitor interacts with this pocket, as well as with the ATP binding site. On the contrary, the first type of inhibitors interacts only with the ATP binding site, formed by the external hinge region and the extra central aromatic ring system, in the active DFG-in conformer [7,8].

Among the computational approaches utilized in drug discovery, pharmacophore-based screening, also known as 3D similarity search, stands out as one of the primary tools employed in ligand-based virtual screening (LBVS) [9]. Alongside molecular docking, molecular dynamics (MD), and three-dimensional quantitative structure–activity relationship (3D-QSAR) analysis, this workflow has been affirmed as one of the most reliable approaches for an optimal structure-based drug design (SBDD) [10-13].

Since VEGF receptor 2 is the subtype primarily responsible for angiogenesis and vasculogenesis, blocking its activity will disrupt the blood supply to tumor cells, thereby impeding their growth, proliferation, and metastasis [7,14]. Furthermore, the disturbed angiogenesis and perturbed vasculogenesis observed in systemic sclerosis (SSc), as well as in other rheumatic diseases like rheumatoid arthritis (RA) [15] and systemic lupus erythematosus (SLE) [16], may be subjected to regulation [17]. All three VEGF receptors (VEGFRs) are upregulated in skin biopsies from patients with systemic sclerosis (SSc), with VEGFR-2 expression particularly increased on endothelial cells, indicating a disruption of the VEGF signaling system [18-20]. In contrast, late-outgrowth endothelial progenitor cells (EPCs) from SSc patients fail to adequately upregulate VEGFR-1 under hypoxic conditions, a defect that may enhance VEGF/VEGFR-2 signaling, leading to persistent VEGF stimulation and contributing to aberrant vascular morphology and function [21]. For these reasons, we employed SBDD approaches,

utilizing the three-dimensional structure of VEGF receptor 2, to explore potential ligands and promote the development of novel drugs with potential affinity for therapeutic targets [22].

Results

Virtual Screening of compound databases

The LBVS, particularly the pharmacophore-based screening, yielded a set of potential ligands (reported in Table 1) with both minimum pharmacophore RMSD value and higher affinity for human VEGFR2 tyrosine kinase, considering the current availability of compound databases. The three-dimensional images in the Figure 1 show a comparison between the pharmacophore model of 00J and those obtained for two of the best-fitting ligands found in the PubChem database, PubChem-143070699 and PubChem-90342547. The features of the first one include a main cluster (circled in black) of two hydrophobic, an aromatic, and a hydrogen acceptor functional group, as previously reported [1], with a further hydrogen donor functional group. The last two are in proximity to the DFG motif. Moreover, this model includes another two hydrophobic and a hydrogen acceptor functional group in proximity of the linker/hinge region, indicated by the arrow. The other two models show additional functional groups, another hydrophobic group in the main cluster and, in the extended hydrophobic pocket, a hydrogen acceptor and a hydrophobic functional group, respectively.

Molecular Docking

The best-fitting ligands identified in the pharmacophore model of compound 00J were subjected to further analysis using two molecular docking algorithms (see methods section), along with the top-performing ligands previously evaluated against the human VEGFR2 tyrosine kinase [12]. The mean affinity values of the complexes, both in term of free energy of binding and in term of predicted equilibrium dissociation constants, are reported in Table 1. The nanomolar/sub-micromolar range of these values indicates a very high affinity of these compounds for human VEGFR2 tyrosine kinase. However, for many of them, there may not be high specificity regarding affinity for human VEGFR2 tyrosine kinase as well (*e.g.* Ag-13958 and Ditercalinium). While synthetic molecules/drugs comprise the majority of compounds with the highest affinity, natural compounds such as luteolin, curcumin, and quercetin also demonstrate medium to high affinities comparable to efficient inhibitors and the substrate ATP (K_m = 5 □M) [23].

To further validate the docking process, we compared the 00J/human VEGFR2 tyrosine kinase and sorafenib/human VEGFR2 tyrosine kinase predicted complexes with the available crystal structure geometries (PDB ID: 2XIR and 3WZE), resulting in a ligand–ligand superimpose RMSD value of 0.57 Å and 0.67 Å, respectively, as previously reported [1]. These values, being significantly lower than 1 Å, indicate a good reliability of the algorithms used. Moreover, when considering the molecules that exhibited identical poses (RMSD < 0.8 Å) and geometries after the two docking procedures, both algorithms demonstrate a high correlation in affinity results (see Figure S1), even though this consistent geometry was not observed for all molecules.

The predicted interactions characterizing the most represented ligand/human VEGFR2 tyrosine kinase complexes are depicted in the Figure 1 (2D representations on the right) and Figure 2. Based on the pharmacophore models, the ligands with the highest affinity (PubChem-143070699, with IUPAC name: 7-fluoro-6-(7-hydroxyquinolin-4-yl)oxy-2-methyl-*N*-(6-morpholin-4-ylpyridin-3-yl)-1-benzofuran-3-carboxamide, and PubChem-90342547, with IUPAC name: 5-(6,7-dimethoxyquinazolin-4-yl)oxy-4-fluoro-2-methyl-*N*-[3-(trifluoromethyl)phenyl]indole-1-carboxamide) demonstrate interactions that most closely fit with these models. While the compound emerged from an unbiased computational prioritization, its scaffold is structurally related to previously reported quinoline-based kinase inhibitors, extensively disclosed in early patent literature as kinase inhibitors targeting angiogenesis-related pathways, including VEGFR2 (e.g., WO2001032651A1 and related patent families). In particular, the identified binding poses consistently reproduce key interaction patterns characteristic of VEGFR2 inhibition. Notably, a hydrogen bond with Asp1046 and hydrophobic/aromatic interactions with Phe1047 within the DFG motif suggest stabilization of the activation loop region, which is known to be critical for kinase activity modulation. In addition, the hydrogen bond with Glu885 and the interaction with Cys919 in the linker/hinge region are consistent with the canonical hinge-binding mode observed in many VEGFR2 inhibitors, contributing to anchoring of the ligand within the ATP-binding site. Furthermore, an extended network of hydrophobic and aromatic contacts involving residues such as Leu840, Val848, Ala866, Lys868, Val916, Phe918, Gly922, and Leu1035 supports ligand accommodation within the hydrophobic pocket and may contribute to binding affinity and specificity. Moreover, the potential hydrophobic/aromatic interactions within the extended hydrophobic pocket (Glu885, Ile888, Leu889, His891, Ile892, and Cys1045) are also noteworthy. For this reason, the other selected ligands, which only exhibit some of the features of this pharmacophore model, are predicted to have a lower affinity for the human VEGFR2 tyrosine kinase (Figure 2). Although the docking box for the EADock DSS algorithm was configured for the entire protein, all complexes exclusively engaged these human VEGFR2 tyrosine kinase active site, suggesting the absence of any alternative binding sites.

Molecular Dynamics

The molecular dynamics simulation was performed to assess the stability of the human VEGFR2 tyrosine kinase binding to PubChem-143070699, Bms-833923, Hispaglabridin_B, and PubChem-146371572, which were selected based on their affinity and binding site. Figure 3 reports the initial ten nanoseconds of the simulation, as no additional RMSD variations were observed beyond this timeframe (see supplementary figures 2-5, box A and B).

Considering complex trajectory with respect to the backbone, all complexes achieve sufficient stability (RMSD value of about 0.35 nm) within less than 3 ns. The trajectory of the PubChem-143070699 molecule, with respect to the backbone, indicates stability was achieved in approximately 6 ns, whereas that of Bms-833923 stabilized in less than 2 ns, with respective RMSD values of 0.4 nm and 0.35 nm (Figure 3A and 3C). The stability of PubChem-146371572 was reached in about 7 ns (RMSD value lower than 0.6 nm), as shown by the trajectory of the

molecule with respect to the backbone. This behavior may be attributed to the molecule's potential inhibitory action, specifically its binding to the ATP binding site of human VEGFR2 tyrosine kinase, characterized as the first type. Conclusively, the binding of Hispaglabridin_B to human VEGFR2 tyrosine kinase exclusively within the extended hydrophobic pocket results in a less stable complex, as demonstrated by MD simulation (RMSD value of about 1.5 nm, Figure 3E) and the lower interaction energy calculated from this analysis (Table 2). This confirms both the quantity and the type of interactions predicted for this complex (Figure 2), allowing the ligand to be exposed to solvent and move freely. The molecular dynamics analysis yielded also the average short-range Coulombic and Lennard–Jones interaction energies, which are documented in Table 2. As outlined in the molecular docking section (regarding hydrophobic/aromatic interactions and predicted hydrogen bonds), all electrostatic contributions are notably lower than the intermolecular pair Lennard–Jones potential. Additionally, for all the MD simulations, the RMSF analysis (supplementary figures 2-5, box C and D) highlights reduced flexibility in key functional regions of human VEGFR2 tyrosine kinase, particularly in the hinge region (Glu917–Cys919) and the catalytic DFG motif (Asp1046–Gly1048). Hydrogen bond analysis further confirms persistent interactions between the ligand and hinge residue Cys919 during the simulation (supplementary figures 2-5, box E). Moreover, the radius of gyration remained stable throughout the trajectory, indicating that ligand binding does not significantly affect the global compactness of the protein (supplementary figures 2-5, box F).

Three-Dimensional Quantitative Structure–Activity Relationship (3D-QSAR) and ADMET Analysis

The comparative molecular fields analysis (CoMFA) models, derived from a complete three-dimensional QSAR analysis, are showcased in Table 3, focusing on the optimal principal components (OPC). From these models, factors such as molecular weight (MW), number of hydrogen bond acceptors (nHA), number of hydrogen bond donors (nHD), logarithm of the n-octanol/water distribution coefficient (LogP), topological polar surface area (TPSA), rotatable bonds (RBs), molar refractivity (MR), length, and max length were properly considered and adjusted to refine the model's accuracy.

In Figure 4, the correlations between experimental and calculated activities by CoMFA models are depicted. Moreover, the OPC has also been raised to 4 to achieve a squared correlation coefficient (r^2) of 0.95. The statistical analysis, detailed in Table 3, reveals that the steric model (STE) demonstrates greater consistency and robustness compared to the electrostatic model (ELE), since ELE displaying a substandard squared correlation coefficient (r^2) and internal predictive coefficient (q^2). This finding aligns with the outcomes of interaction energies derived from Gromacs energy module and with the pharmacophore best model, which highlight the complex with the highest Lennard-Jones energy contribution as possessing the greatest affinity, indicative of the predominant role of steric effects in shaping molecular interactions.

ADMET predictions, including selected properties and associated descriptors for the 53 compounds, are reported in Supplementary Table 1. Most compounds satisfied the acceptance

criteria for the Lipinski and Pfizer indices, which are related to absorption, permeability and toxicity. Only PubChem-158796309 failed to meet these criteria.

Discussion

As a factor pivotal in regulating endothelial cell proliferation, migration, survival, and new blood vessels formation, VEGF receptor 2 has been identified in numerous studies as a potential target for treating conditions such as cancer and progressive fibrotic diseases [7,14,18,19,21]. This is achieved through the search for synthetic or natural compounds serving as ligands/inhibitors. However, the exploration of extensive compound libraries, such as those available through the Pharmit server, has yet to be undertaken in this context.

Using molecular docking followed by molecular dynamics simulations, the binding interactions between human intracellular VEGF receptor 2 and compounds selected through pharmacophore-based virtual screening were unveiled. In addition to revealing the affinities of the complexes, molecular docking analysis contributed to elucidating crucial geometrical considerations. The predicted affinities for the 53 studied complexes range from the nanomolar level (*e.g.*, 1.32 nM for the PubChem-143070699/human VEGFR2 tyrosine kinase complex) to the micromolar level, representing a typical spectrum of values indicative of effective drug inhibition and dependable QSAR analysis. The most stable complexes exhibit interactions that closely align with the pharmacophore features, thus confirming the validity of the proposed model. Although PubChem-143070699 was identified as a top candidate in our computational screening, its chemical scaffold is not entirely unprecedented. A closely related 7-methoxyquinoline analogue has been previously disclosed in the kinase inhibitor patent literature, including compounds with reported VEGFR2 activity. Therefore, the significance of our findings lies not in the identification of a novel chemotype per se, but in the independent computational prioritization of this scaffold and its predicted binding features within the VEGFR2 active site. This supports the robustness of the screening workflow and highlights its ability to recover biologically relevant chemical space.

Analysis using molecular dynamics (MD) indicates that the complexes rapidly attain stability and maintain it throughout all MD simulations, with no significant unfolding of the structures observed. Overall, the extended and replicated MD simulations support the dynamic persistence of the ligand–protein interactions, although the degree of conformational stability differs among complexes. An exception is related to the complex that exclusively comprises the involvement of the extended hydrophobic pocket (*e.g.*, Hispaglabridin_B/hiVEGFR2 complex that shows lower stability than the other systems). During this analysis, the calculated interaction energies indicate that the steric contribution (the Lennard–Jones energy) predominates in all complexes. This observation is corroborated by CoMFA models derived from three-dimensional QSAR. Because the CoMFA model was developed using activity values estimated from docking scores rather than experimental biological data, the resulting correlations should be interpreted with caution. Moreover, the relatively small and structurally homogeneous dataset limits the robustness and generalizability of the model; therefore, the

identified steric/electrostatic features should be considered preliminary and mainly applicable within the chemical space explored in this study. The q^2 values obtained for the CoMFA models were low, indicating limited internal predictive robustness. This may be due to the relatively small size of the dataset, possible heterogeneity in the biological data, the narrow activity range of some compounds, and the well-known sensitivity of CoMFA models to molecular alignment. Consequently, the model should be regarded as providing qualitative SAR information rather than a robust predictive framework. The steric model field yields a highly reliable activity predictor, hinting at the significance of descriptors within this field and the structural insights gleaned from molecular docking analysis for designing novel, efficacious drugs. The molecule ranking reported in Table 1 is confirmed by these predicted models and structural information, pinpointing PubChem-143070699 as the suitable candidate for a human VEGFR2 tyrosine kinase ligand/inhibitor.

Although reliant on bioinformatics tools and awaiting experimental validation, this analysis posits the potential to establish a platform for the development of novel drugs or the repurposing of existing ones. While the projected model serves as a robust foundation for the development of an optimal human VEGFR2 tyrosine kinase ligand/inhibitor, all 53 selected compounds demonstrate the potential to effectively bind and inhibit human VEGFR2 tyrosine kinase activity, as evidenced by their predicted geometries and affinities. The fact that compounds such as Sorafenib, Sunitinib, PF-210 (or 00j), Cabozantinib, Semaxanib, and Nintedanib - all belonging to this set - have already demonstrated *in vitro* activity against human VEGFR2 tyrosine kinase partially reinforces these concepts [1,3,4,24-32], even if the affinity values reported in these studies are not always consistent with those stated here.

Further research is necessary to determine if these compounds, especially those exclusively listed as PubChem members and exhibiting a higher affinity for human VEGFR2 tyrosine kinase, merit advancement to the pre-clinical and clinical evaluation stages. Although multiple small-molecule inhibitors of the VEGFR2 are approved for the treatment of different type of cancers, their toxicity and wide range of side effects remain a critical issue, leading to short-lived clinical effects and treatment failures. Tyrosine kinase inhibitors targeting VEGFR2, such as Nintedanib [33-36], are also becoming increasingly important for non-neoplastic disorders, such as fibrotic diseases. In this context, it is imperative to meticulously calibrate the dosages of these novel medications in real-world contexts to ensure optimal efficacy and safety for patients. Close monitoring of potential side effects and effective collaboration between healthcare providers and patients are necessary to adjust treatment appropriately, considering individual patient clinical factors.

Online Methods

Virtual Screening of compound databases

Pharmacophore search modalities are used to perform virtual screening of large pre-built libraries of popular compound databases using the Pharmit server [37]. Currently, the 11 pre-built libraries, generated in Pharmit from databases such as PubChem [38] and MolPort

(www.molport.com), along with approximately 2.200 publicly accessible user-contributed libraries, contain about 450 million compounds. Starting from the crystallographic structure with PDB ID: 2XIR of human intracellular VEGFR2 complexed with PF-00337210 (the oral and highly selective VEGFR inhibitor also known as PF-210 or 00J [29]), which is considered the best available crystallographic structure in terms of resolution (1.50 Å), the server generated a list of compounds aligned to the 00J pharmacophore. These compounds were sorted based on their pharmacophore root mean square deviation (RMSD) and subjected to energy minimization using AutoDock Vina [39] scoring function and smina [40], a fork of Vina with enhanced minimization functionality. This list was finally completed to a total of 53 compounds with the set of ligands that had previously shown the best affinity for the analogous human intracellular platelet-derived growth factor receptor alpha [12].

Molecular Docking

To assess the ranking obtained from the virtual screening, we performed a further molecular docking analysis using both Autodock Vina software [39], based on the genetic algorithm, and SwissDock web server [41], based on the EADock DSS algorithm. For the first one, the grid center coordinates (19.287, 21.244, 36.624) and the size of the docking box (30 □ 26 □ 24 Å) were fixed, while for the second one, the docking type was set as accurate without defining the region of interest to encompass the entire protein within the search space. All the other parameters were set as default. Predicted equilibrium dissociation constants ($K_{d,pred}$) of complexes were calculated from the mean of the free energy of binding (ΔG) obtained from the two algorithms and using the standard equation $K_{D,pred} = e^{\Delta G \frac{1000}{RT}}$.

The final geometry of the complexes obtained with the pharmacophore visualization was rendered on the Pharmit server [37] and the 2D representation of the interaction was obtained by the PoseEdit tool [42] available in the ProteinsPlus server [43].

Molecular Dynamics

Gromacs software version 2023.1 [44] alongside the CHARMM36 force field updated July 2022 [45], the SPC216 water model, and the CGenFF server for generating ligand topologies [45], was utilized to conduct the molecular dynamics (MD) simulations of four ligand/receptor complexes selected based of different $K_{d,pred}$ values and ligand geometries. The initiation of each dynamics simulation involved solvation, neutralization with the addition of six chlorine ions, and system minimization using the steepest descent algorithm over 50,000 steps. Then, the NVT and NPT equilibration stage was performed in a 100 ps run, stabilizing the temperature at 300 K (using V-rescale Berendsen thermostat) and the pressure at 1 bar (using C-rescale pressure coupling), respectively. Ultimately, MD simulation was conducted over a 50 ns duration, employing Gromacs' RMS tools to ascertain the root mean square deviation (RMSD) for every ligand trajectory concerning the protein backbone. Furthermore, the protein backbone RMSD was computed relative to the energy-minimized conformation, including RMSF, radius of gyration, hydrogen bond occupancy, and ligand–protein contact persistence. The Coulombic and

Lennard–Jones interaction energies were calculated using the capability of Gromacs to decompose the short-range non-bonded energies. In addition, three independent replicate simulations were carried out for each system using the same protocol and different initial velocity distributions.

Three-Dimensional Quantitative Structure–Activity Relationship (3D-QSAR) and ADMET Analysis

To streamline the development of targeted intracellular VEGFR2 inhibitors in humans, we conducted a three-dimensional quantitative structure–activity relationship (3D-QSAR) analysis using the comparative molecular fields analysis (CoMFA) [46] tool, accessible via the web portal www.3d-qsar.com [47]. In this analysis, we initially aligned the conformations of the molecules and calculated molecular interaction fields (MIFs) for the 53 selected compounds, using default parameters. The dataset of 53 compounds was divided into a training set of 15 compounds and a test set of 38 compounds. The test compounds were selected to ensure representation of both the structural diversity of the series and the full range of biological activity values. Internal validation was performed by leave-one-out (LOO) cross-validation to obtain q^2 values, while external predictivity was assessed using the test set. The resulting CoMFA potentials, termed steric (STE) and electrostatic (ELE), were derived from Lennard–Jones and Coulomb law definitions, respectively.

ADMET (absorption, distribution, metabolism, excretion and toxicity) properties were evaluated using the screening module of the ADMETlab 3.0 web server [48] by uploading the SMILES strings of the 53 selected molecules. In addition to standard molecular descriptors, four acceptance indices (Lipinski, Pfizer, GSK and Golden Triangle) were calculated. The Lipinski criteria relate to absorption and permeability, whereas the Pfizer rule is associated with toxicity. Compounds meeting the GSK and Golden Triangle criteria are expected to exhibit a more favourable ADMET profile.

References

1 Sobhy, M. K., Mowafy, S., Lasheen, D. S., Farag, N. A. & Abouzid, K. A. M. 3D-QSAR pharmacophore modelling, virtual screening and docking studies for lead discovery of a novel scaffold for VEGFR 2 inhibitors: Design, synthesis and biological evaluation. *Bioorg Chem* **89**, 102988 (2019). https://doi.org:10.1016/j.bioorg.2019.102988

2 Abhinand, C. S., Raju, R., Soumya, S. J., Arya, P. S. & Sudhakaran, P. R. VEGF-A/VEGFR2 signaling network in endothelial cells relevant to angiogenesis. *J Cell Commun Signal* **10**, 347-354 (2016). https://doi.org:10.1007/s12079-016-0352-8

3 Machado, V. A. *et al.* Synthesis, antiangiogenesis evaluation and molecular docking studies of 1-aryl-3-[(thieno[3,2-b]pyridin-7-ylthio)phenyl]ureas: Discovery of a new substitution pattern for type II VEGFR-2 Tyr kinase inhibitors. *Bioorg Med Chem* **23**, 6497-6509 (2015). https://doi.org:10.1016/j.bmc.2015.08.010

4 Musumeci, F., Radi, M., Brullo, C. & Schenone, S. Vascular endothelial growth factor (VEGF) receptors: drugs and new inhibitors. *J Med Chem* **55**, 10797-10822 (2012). https://doi.org:10.1021/jm301085w

5 Lee, C. *et al.* Vascular endothelial growth factor signaling in health and disease: from molecular mechanisms to therapeutic perspectives. *Signal Transduct Target Ther* **10**, 170 (2025). https://doi.org:10.1038/s41392-025-02249-0

6 Zeng, J. *et al.* Recent development of VEGFR small molecule inhibitors as anticancer agents: A patent review (2021-2023). *Bioorg Chem* **146**, 107278 (2024). https://doi.org:10.1016/j.bioorg.2024.107278

7 Elsayed, N. M. Y. *et al.* Design, synthesis, biological evaluation and dynamics simulation of indazole derivatives with antiangiogenic and antiproliferative anticancer activity. *Bioorg Chem* **82**, 340-359 (2019). https://doi.org:10.1016/j.bioorg.2018.10.071

8 Shahin, M. I., Abou El Ella, D. A., Ismail, N. S. & Abouzid, K. A. Design, synthesis and biological evaluation of type-II VEGFR-2 inhibitors based on quinoxaline scaffold. *Bioorg Chem* **56**, 16-26 (2014). https://doi.org:10.1016/j.bioorg.2014.05.010

9 Singh, N., Chaput, L. & Villoutreix, B. O. Virtual screening web servers: designing chemical probes and drug candidates in the cyberspace. *Brief Bioinform* **22**, 1790-1818 (2021). https://doi.org:10.1093/bib/bbaa034

10 Salem, M. S. H., Abdel Aziz, Y. M., Elgawish, M. S., Said, M. M. & Abouzid, K. A. M. Design, synthesis, biological evaluation and molecular modeling study of new thieno[2,3-d]pyrimidines with anti-proliferative activity on pancreatic cancer cell lines. *Bioorg Chem* **94**, 103472 (2020). https://doi.org:10.1016/j.bioorg.2019.103472

11 Ejaz, S. A., Aziz, M., Fawzy Ramadan, M., Fayyaz, A. & Bilal, M. S. Pharmacophore-Based Virtual Screening and In-Silico Explorations of Biomolecules (Curcumin Derivatives) of Curcuma longa as Potential Lead Inhibitors of ERBB and VEGFR-2 for the Treatment of Colorectal Cancer. *Molecules* **28** (2023). https://doi.org:10.3390/molecules28104044

12 Mozzicafreddo, M. *et al.* Screening and Analysis of Possible Drugs Binding to PDGFRalpha: A Molecular Modeling Study. *Int J Mol Sci* **24** (2023). https://doi.org:10.3390/ijms24119623

13 Dong, J. & Hao, X. Pharmacophore screening, molecular docking, and MD simulations for identification of VEGFR-2 and c-Met potential dual inhibitors. *Front Pharmacol* **16**, 1534707 (2025). https://doi.org:10.3389/fphar.2025.1534707

14 Rajagopalan, M., Balasubramanian, S., Ramaswamy, A. & Mathur, P. P. Pharmacophore based 3D-QSAR modeling and free energy analysis of VEGFR-2 inhibitors. *J Enzyme Inhib Med Chem* **28**, 1236-1246 (2013). https://doi.org:10.3109/14756366.2012.729826

15 Marrelli, A. *et al.* Angiogenesis in rheumatoid arthritis: a disease specific process or a common response to chronic inflammation? *Autoimmun Rev* **10**, 595-598 (2011). https://doi.org:10.1016/j.autrev.2011.04.020

16 Denny, M. F. *et al.* Interferon-alpha promotes abnormal vasculogenesis in lupus: a potential pathway for premature atherosclerosis. *Blood* **110**, 2907-2915 (2007). https://doi.org:10.1182/blood-2007-05-089086

17 Zhang, Y. & Distler, J. H. Therapeutic molecular targets of SSc-ILD. *J Scleroderma Relat Disord* **5**, 17-30 (2020). https://doi.org:10.1177/2397198319899013

18 Distler, O. *et al.* Uncontrolled expression of vascular endothelial growth factor and its receptors leads to insufficient skin angiogenesis in patients with systemic sclerosis. *Circ Res* **95**, 109-116 (2004). https://doi.org:10.1161/01.RES.0000134644.89917.96

19 Higashi-Kuwata, N., Makino, T., Inoue, Y. & Ihn, H. Expression pattern of VEGFR-1, -2, -3 and D2-40 protein in the skin of patients with systemic sclerosis. *Eur J Dermatol* **21**, 490-494 (2011). https://doi.org:10.1684/ejd.2011.1284

20 Zaccone, V. *et al.* Systemic Sclerosis: A Key Model of Endothelial Dysfunction. *Biomedicines* **13** (2025). https://doi.org:10.3390/biomedicines13071771

21 Avouac, J. *et al.* Angiogenesis in systemic sclerosis: impaired expression of vascular endothelial growth factor receptor 1 in endothelial progenitor-derived cells under hypoxic conditions. *Arthritis Rheum* **58**, 3550-3561 (2008). https://doi.org:10.1002/art.23968

22 Zinellu, A. & Mangoni, A. A. Vascular endothelial growth factor as a potential biomarker in systemic sclerosis: a systematic review and meta-analysis. *Front Immunol* **15**, 1442913 (2024). https://doi.org:10.3389/fimmu.2024.1442913

23 Carey, K. D. *et al.* Kinetic analysis of epidermal growth factor receptor somatic mutant proteins shows increased sensitivity to the epidermal growth factor receptor tyrosine kinase inhibitor, erlotinib. *Cancer Res* **66**, 8163-8171 (2006). https://doi.org:10.1158/0008-5472.CAN-06-0453

24 Mendel, D. B. *et al.* In vivo antitumor activity of SU11248, a novel tyrosine kinase inhibitor targeting vascular endothelial growth factor and platelet-derived growth

factor receptors: determination of a pharmacokinetic/pharmacodynamic relationship. *Clin Cancer Res* **9**, 327-337 (2003).

25 Roskoski, R., Jr. Sunitinib: a VEGF and PDGF receptor protein kinase and angiogenesis inhibitor. *Biochem Biophys Res Commun* **356**, 323-328 (2007). https://doi.org:10.1016/j.bbrc.2007.02.156

26 Wilhelm, S. *et al.* Discovery and development of sorafenib: a multikinase inhibitor for treating cancer. *Nat Rev Drug Discov* **5**, 835-844 (2006). https://doi.org:10.1038/nrd2130

27 Fong, T. A. *et al.* SU5416 is a potent and selective inhibitor of the vascular endothelial growth factor receptor (Flk-1/KDR) that inhibits tyrosine kinase catalysis, tumor vascularization, and growth of multiple tumor types. *Cancer Res* **59**, 99-106 (1999).

28 Sun, L. *et al.* Design, synthesis, and evaluations of substituted 3-[(3- or 4-carboxyethylpyrrol-2-yl)methylidenyl]indolin-2-ones as inhibitors of VEGF, FGF, and PDGF receptor tyrosine kinases. *J Med Chem* **42**, 5120-5130 (1999). https://doi.org:10.1021/jm9904295

29 Majeti, B. K., Lee, J. H., Simmons, B. H. & Shojaei, F. VEGF is an important mediator of tumor angiogenesis in malignant lesions in a genetically engineered mouse model of lung adenocarcinoma. *BMC Cancer* **13**, 213 (2013). https://doi.org:10.1186/1471-2407-13-213

30 Amantini, C. *et al.* Sorafenib induces cathepsin B-mediated apoptosis of bladder cancer cells by regulating the Akt/PTEN pathway. The Akt inhibitor, perifosine, enhances the sorafenib-induced cytotoxicity against bladder cancer cells. *Oncoscience* **2**, 395-409 (2015). https://doi.org:10.18632/oncoscience.147

31 Santoni, M. *et al.* Pazopanib and sunitinib trigger autophagic and non-autophagic death of bladder tumour cells. *Br J Cancer* **109**, 1040-1050 (2013). https://doi.org:10.1038/bjc.2013.420

32 Allanore, Y. *et al.* Continued nintedanib in patients with systemic sclerosis-associated interstitial lung disease: 3-year data from SENSCIS-ON. *RMD Open* **11** (2025). https://doi.org:10.1136/rmdopen-2024-005086

33 Campochiaro, C. *et al.* Real-life efficacy and safety of nintedanib in systemic sclerosis-interstitial lung disease: data from an Italian multicentre study. *RMD Open* **9** (2023). https://doi.org:10.1136/rmdopen-2022-002850

34 Cutolo, M. *et al.* Nintedanib downregulates the transition of cultured systemic sclerosis fibrocytes into myofibroblasts and their pro-fibrotic activity. *Arthritis Res Ther* **23**, 205 (2021). https://doi.org:10.1186/s13075-021-02555-2

35 Distler, O. *et al.* Nintedanib for Systemic Sclerosis-Associated Interstitial Lung Disease. *N Engl J Med* **380**, 2518-2528 (2019). https://doi.org:10.1056/NEJMoa1903076

36 Huang, J. *et al.* Nintedanib inhibits fibroblast activation and ameliorates fibrosis in preclinical models of systemic sclerosis. *Ann Rheum Dis* **75**, 883-890 (2016). https://doi.org:10.1136/annrheumdis-2014-207109

37 Sunseri, J. & Koes, D. R. Pharmit: interactive exploration of chemical space. *Nucleic Acids Res* **44**, W442-448 (2016). https://doi.org:10.1093/nar/gkw287

38 Kim, S. *et al.* PubChem Substance and Compound databases. *Nucleic Acids Res* **44**, D1202-1213 (2016). https://doi.org:10.1093/nar/gkv951

39 Trott, O. & Olson, A. J. AutoDock Vina: improving the speed and accuracy of docking with a new scoring function, efficient optimization, and multithreading. *J Comput Chem* **31**, 455-461 (2010). https://doi.org:10.1002/jcc.21334

40 Koes, D. R., Baumgartner, M. P. & Camacho, C. J. Lessons learned in empirical scoring with smina from the CSAR 2011 benchmarking exercise. *J Chem Inf Model* **53**, 1893-1904 (2013). https://doi.org:10.1021/ci300604z

41 Grosdidier, A., Zoete, V. & Michielin, O. SwissDock, a protein-small molecule docking web service based on EADock DSS. *Nucleic Acids Res* **39**, W270-277 (2011). https://doi.org:10.1093/nar/gkr366

42 Diedrich, K., Krause, B., Berg, O. & Rarey, M. PoseEdit: enhanced ligand binding mode communication by interactive 2D diagrams. *J Comput Aided Mol Des* **37**, 491-503 (2023). https://doi.org:10.1007/s10822-023-00522-4

43 Schoning-Stierand, K. *et al.* ProteinsPlus: a comprehensive collection of web-based molecular modeling tools. *Nucleic Acids Res* **50**, W611-W615 (2022). https://doi.org:10.1093/nar/gkac305

44 Van Der Spoel, D. *et al.* GROMACS: fast, flexible, and free. *J Comput Chem* **26**, 1701-1718 (2005). https://doi.org:10.1002/jcc.20291

45 Vanommeslaeghe, K. *et al.* CHARMM general force field: A force field for drug-like molecules compatible with the CHARMM all-atom additive biological force fields. *J Comput Chem* **31**, 671-690 (2010). https://doi.org:10.1002/jcc.21367

46 Cramer, R. D., Patterson, D. E. & Bunce, J. D. Comparative molecular field analysis (CoMFA). 1. Effect of shape on binding of steroids to carrier proteins. *J Am Chem Soc* **110**, 5959-5967 (1988). https://doi.org:10.1021/ja00226a005

47 Ragno, R. www.3d-qsar.com: a web portal that brings 3-D QSAR to all electronic devices-the Py-CoMFA web application as tool to build models from pre-aligned datasets. *J Comput Aided Mol Des* **33**, 855-864 (2019). https://doi.org:10.1007/s10822-019-00231-x

48 Fu, L. *et al.* ADMETlab 3.0: an updated comprehensive online ADMET prediction platform enhanced with broader coverage, improved performance, API functionality and decision support. *Nucleic Acids Res* **52**, W422-W431 (2024). https://doi.org:10.1093/nar/gkae236

Funding

This research has received funding from the project Heal Italia – Project Code PE00000019, CUP I33C22006900006 - funded under the National Recovery and Resilience Plan (NRRP), Mission 4 Component 2 Investment 1.3 - Creation of "Extended Partnerships with Universities, Research Centers, and Companies for the Funding of Basic Research Projects" – Project "Health Extended Alliance for Innovative Therapies, Advanced Lab Research, and Integrated Approaches of Precision Medicine (HEAL ITALIA)" Call for tender No. 341 of 15/03/2022, and Concession Decree No. 0001559.11-10-2022 of Italian Ministry of University funded by the European Union – NextGenerationEU.

Author Contributions

M.M. and G.M. conceived the idea. M.M. performed conceptualization and method development, method validation, software curation, data management, and preparation of the original draft. All authors contributed to manuscript revision and approved the submitted version.

Figures

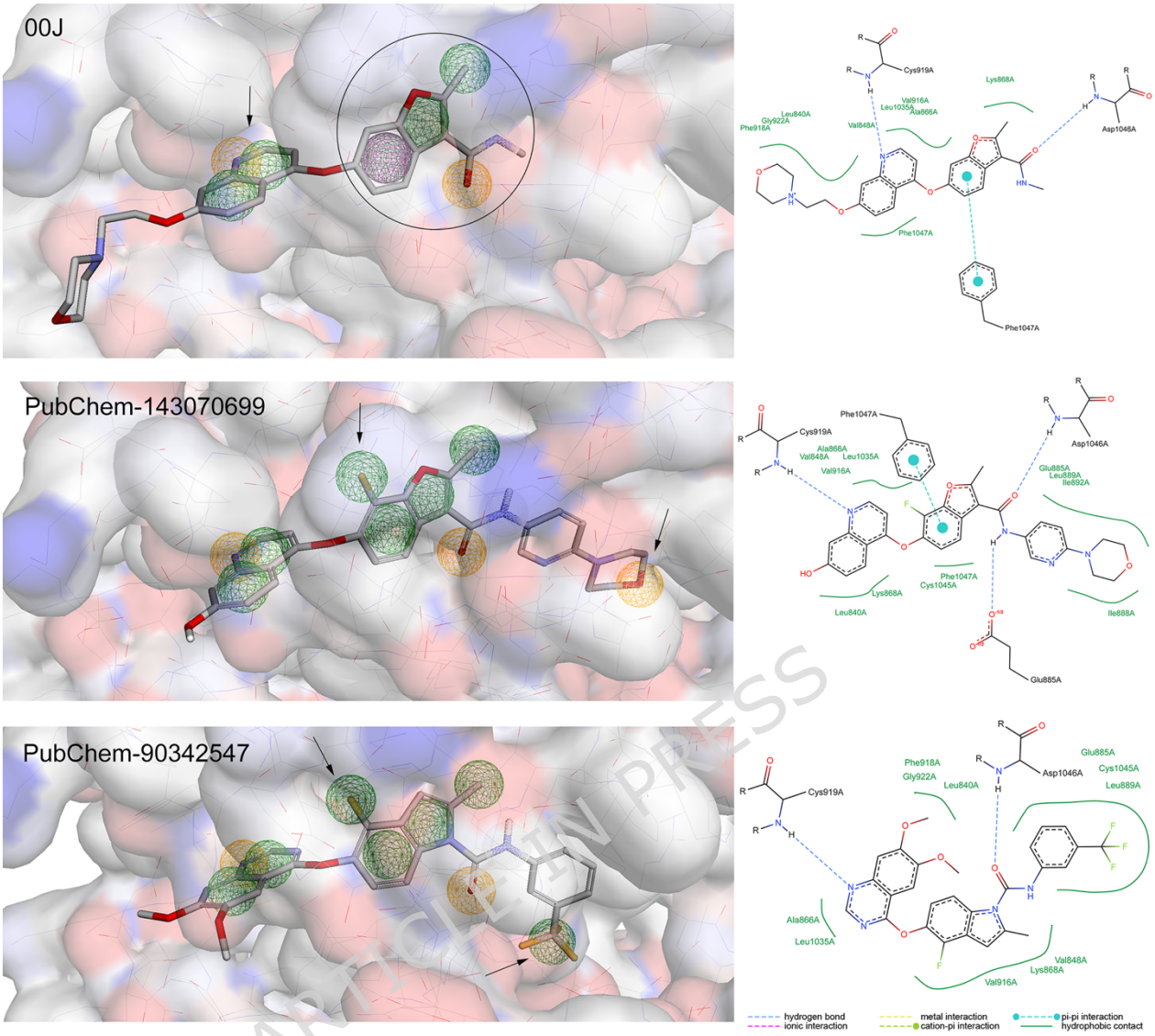

Figure 1 – Three-dimensional representations and pharmacophore models of the molecule complexed with human VEGFR2 tyrosine kinase (00J, PubChem-143070699 and PubChem-90342547) are shown in the panels. The functional groups are color-coded as follows: aromatic in violet, hydrophobic in green, hydrogen donor in white, and hydrogen acceptor in yellow. Two-dimensional representations of the same complexes and the corresponding legend describing the types of interactions are displayed in the right panels.

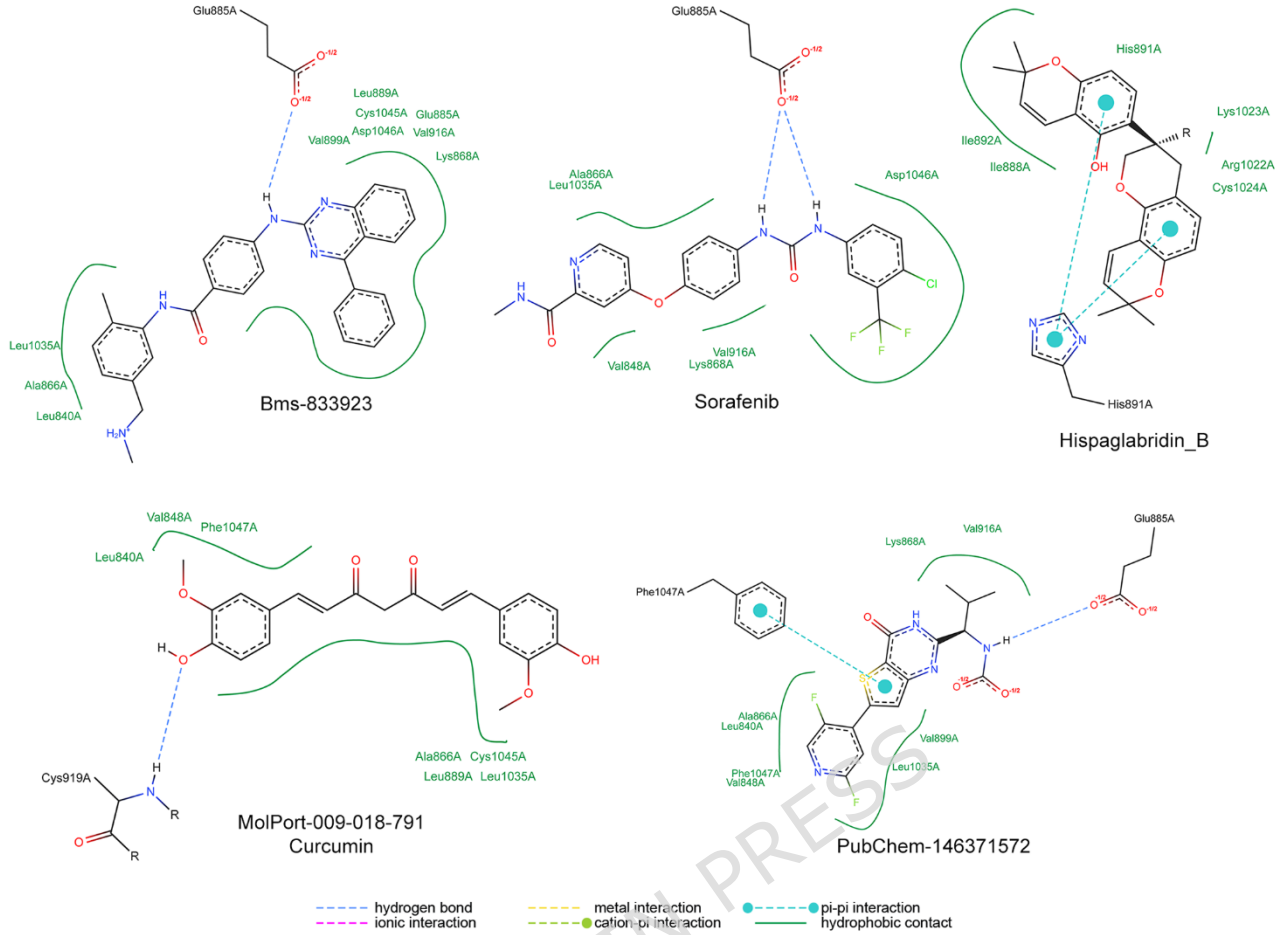

Figure 2 - Two-dimensional representations of additional complexes identified in the Results and Discussion section, along with their corresponding legends describing the types of interactions.

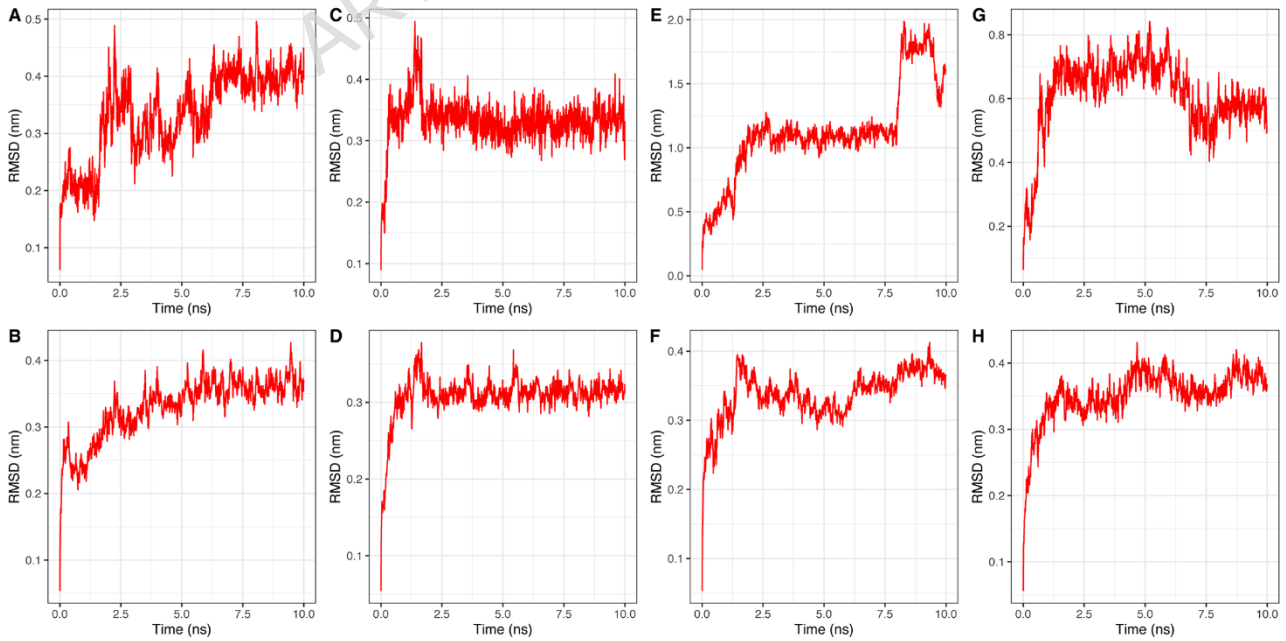

Figure 3 - RMSDs of ligands and complexes trajectories: (A,C,E,G) RMSDs of PubChem-143070699, Bms-833923, Hispaglabridin_B, and PubChem-146371572 versus protein backbone, respectively; (B,D,F,H) RMSDs of human VEGFR2 tyrosine kinase versus protein

backbone complexed with PubChem-143070699, Bms-833923, Hispaglabridin_B, and PubChem-146371572, respectively.

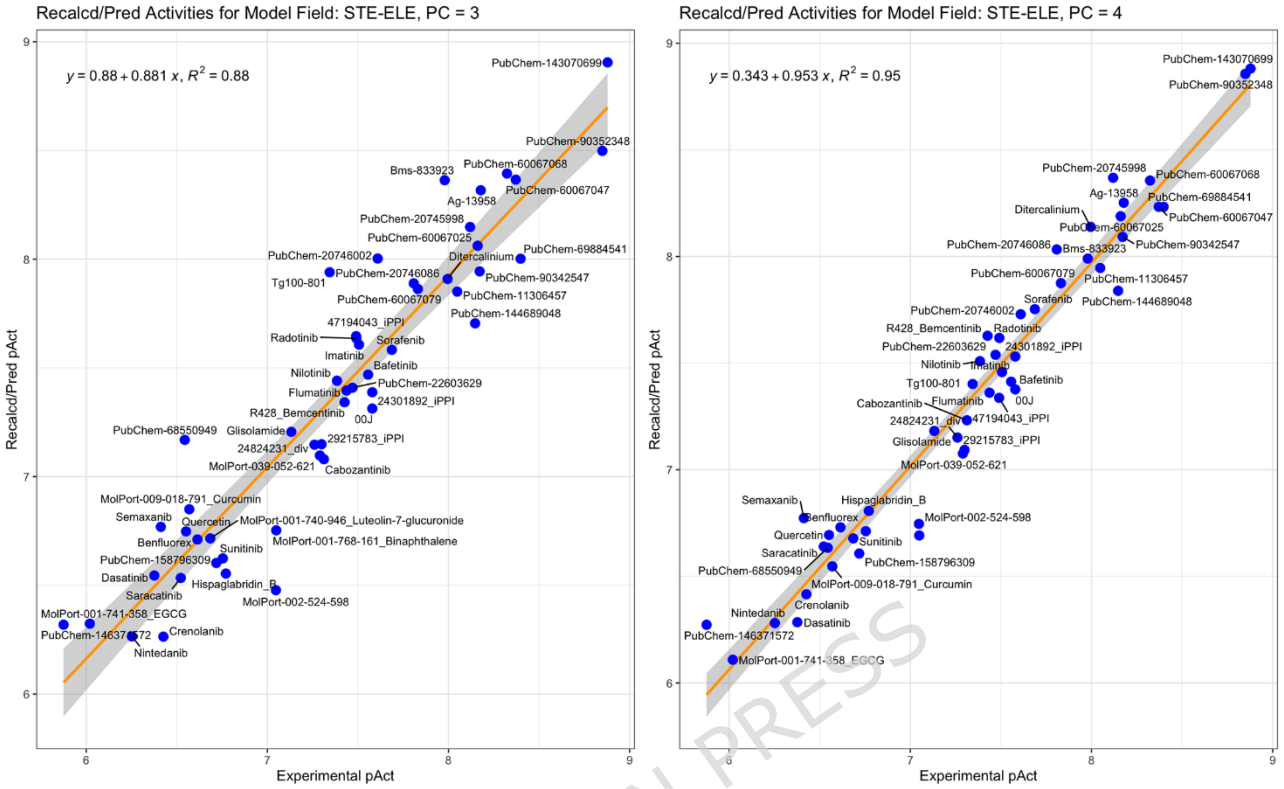

Figure 4 – Linear relationship between the predicted activity values (Recalcd/Pred pAct) generated by the CoMFA model with experimental activities derived from molecular docking analysis, taking into account the PC values.

Tables

Table I - The best compounds selected after the pharmacophore-based virtual screening and their affinities for the human VEGFR2 tyrosine kinase achieved after the molecular docking analysis. Here, the *ΔG* values are reported as means and standard errors, analyzed using the two docking algorithms described in the methods section.

Compound	*ΔG* mean (kcal/mol)	*ΔG* mean (kJ/mol)	$K_{d,pred}$ (M)
PubChem-143070699	-12.10 ± 1.30	-50,63 ± 5.84	1.32 ± 10^{-09}
PubChem-90352348	-12.06 ± 1.02	-50.46 ± 4.27	1.42 ± 10^{-09}
PubChem-69884541	-11.45 ± 0.46	-47.91 ± 1.92	3.99 ± 10^{-09}
PubChem-60067047	-11.41 ± 0.12	-47.74 ± 0.50	4.26 ± 10^{-09}
PubChem-60067068	-11.35 ± 0.13	-47.49 ± 0.54	4.75 ± 10^{-09}
PubChem-88037281	-11.15 ± 0.02	-46.65 ± 0.08	6.58 ± 10^{-09}
Ag-13958	-11.15 ± 1.39	-46.65 ± 5.82	6.63 ± 10^{-09}
PubChem-90342547	-11.14 ± 2.02	-46.61 ± 8.45	6.72 ± 10^{-09}
PubChem-60067025	-11.13 ± 0.35	-46.57 ± 1.46	6.91 ± 10^{-09}
PubChem-144689048	-11.11 ± 1.76	-46.48 ± 7.36	7.12 ± 10^{-09}
PubChem-20745998	-11.07 ± 0.06	-46.32 ± 0.25	7.61 ± 10^{-09}
PubChem-11306457	-10.97 ± 0.58	-45.90 ± 2.43	8.95 ± 10^{-09}
Ditercalinium	-10.90 ± 0.92	-45.61 ± 3.85	1.01 ± 10^{-08}
Bms-833923	-10.88 ± 0.94	-45.52 ± 3.93	1.05 ± 10^{-08}
PubChem-60067079	-10.68 ± 0.15	-44.68 ± 0.63	1.48 ± 10^{-08}

PubChem-20746086	-10.64 ± 0.59	-44.52 ± 2.47	1.56 ± 10^{-08}
Sorafenib	-10.48 ± 0.10	-43.85 ± 0.42	2.06 ± 10^{-08}
PubChem-20746002	-10.37 ± 0.89	-43.39 ± 3.72	2.46 ± 10^{-08}
24301892_iPPI/PubChem-15993809	-10.33 ± 1.41	-43.22 ± 5.90	2.63 ± 10^{-08}
00J	-10.33 ± 1.20	-43.22 ± 5.02	2.64 ± 10^{-08}
Bafetinib	-10.30 ± 0.04	-43.09 ± 0.17	2.78 ± 10^{-08}
Imatinib	-10.23 ± 0.67	-42.80 ± 2.80	3.12 ± 10^{-08}
Radotinib	-10.21 ± 1.01	-42.72 ± 4.23	3.23 ± 10^{-08}
47194043_iPPI/PubChem-16727383	-10.21 ± 1.86	-42.72 ± 7.78	3.23 ± 10^{-08}
PubChem-22603629	-10.18 ± 1.70	-42.59 ± 7.11	3.39 ± 10^{-08}
Flumatinib	-10.14 ± 0.29	-42.43 ± 1.21	3.66 ± 10^{-08}
R428_Bemcentinib	-10.12 ± 1.21	-42.34 ± 5.06	3.75 ± 10^{-08}
Nilotinib	-10.07 ± 1.06	-42.13 ± 4.43	4.13 ± 10^{-08}
Tg100-801	-10.01 ± 0.59	-41.88 ± 2.47	4.52 ± 10^{-08}
Cabozantinib	-9.97 ± 0.74	-41.71 ± 3.10	4.88 ± 10^{-08}
29215783_iPPI/PubChem-6540187	-9.95 ± 1.72	-41.63 ± 7.20	5.03 ± 10^{-08}
MolPort-039-052-621	-9.94 ± 1.09	-41.59 ± 4.56	5.12 ± 10^{-08}
PubChem-90352341	-9.93 ± 1.60	-41.55 ± 6.69	5.17 ± 10^{-08}
24824231_div/CHEMBL1331630	-9.90 ± 1.13	-41.42 ± 4.73	5.50 ± 10^{-08}
Glisolamide	-9.72 ± 0.38	-40.67 ± 1.59	7.39 ± 10^{-08}
MolPort-001-768-161_Binaphthalene	-9.61 ± 2.19	-40.21 ± 9.16	8.93 ± 10^{-08}
MolPort-002-524-598	-9.61 ± 0.81	-40.21 ± 3.39	8.97 ± 10^{-08}
Hispaglabridin_B	-9.23 ± 1.74	-38.62 ± 7.28	1.69 ± 10^{-07}
PubChem-144689145	-9.21 ± 0.01	-38.53 ± 0.04	1.76 ± 10^{-07}
Sunitinib	-9.21 ± 0.51	-38.53 ± 2.13	1.76 ± 10^{-07}
PubChem-158796309	-9.16 ± 0.77	-38.32 ± 3.22	1.91 ± 10^{-07}
MolPort-001-740-946_luteolin-7-O-glucuronide	-9.11 ± 0.70	-38.12 ± 2.93	2.07 ± 10^{-07}
Benfluorex	-9.02 ± 0.59	-37.74 ± 2.47	2.43 ± 10^{-07}
MolPort-009-018-791_Curcumin	-8.96 ± 0.12	-37.49 ± 0.50	2.70 ± 10^{-07}
Quercetin	-8.93 ± 1.10	-37.36 ± 4.60	2.81 ± 10^{-07}
PubChem-68550949	-8.92 ± 0.31	-37.32 ± 1.30	2.86 ± 10^{-07}
Saracatinib	-8.89 ± 0.03	-37.20 ± 0.12	3.00 ± 10^{-07}
Crenolanib	-8.76 ± 0.01	-36.65 ± 0.04	3.75 ± 10^{-07}
Semaxanib	-8.74 ± 0.67	-36.57 ± 2.80	3.87 ± 10^{-07}
Dasatinib	-8.69 ± 0.34	-36.36 ± 1.42	4.21 ± 10^{-07}
Nintedanib	-8.52 ± 0.16	-35.65 ± 0.67	5.60 ± 10^{-07}
MolPort-001-741-358_EGCG	-8.21 ± 0.36	-34.35 ± 1.51	9.55 ± 10^{-07}
PubChem-146371572	-8.01 ± 0.29	-33.51 ± 1.21	1.33 ± 10^{-06}

Table II - Average short-range interaction energies were computed using the energy module of Gromacs.

Complex	Coulombic Interaction Energy (kJ/mol)	Lennard-Jones Energy (kJ/mol)
PubChem-143070699 / hiVEGFR2	-32.26 ± 2.50	-184.37 ± 6.00
Bms-833923 / hiVEGFR2	-25.45 ± 4.30	-207.03 ± 9.20
Hispaglabridin_B / hiVEGFR2	-26.44 ± 5.10	-115.02 ± 5.70
PubChem-146371572 / hiVEGFR2	-37.14 ± 3.50	-122.22 ± 1.90

Table III - Summary of the best CoMFA models. Within the brackets, additional values are reported for the model with an increased OPC.

Field	r^2	q^2	Optimal PC
STE	0.885 (0.938)	0.352 (0.202)	2 (3)
ELE	0.012	-0.124	1
STE + ELE	0.880 (0.953)	0.018 (0.008)	3 (4)